

Influence of Welding Combined Plastic Forming on Microstructure Stability and Mechanical Properties of Friction Stir-Welded Al-Cu Alloy

Z.L. Hu, M.L. Dai, and Q. Pang

(Submitted October 31, 2017; in revised form March 23, 2018; published online July 3, 2018)

A new tailor-welded process, which combines stages of welding, plastic forming, and heat treatment strengthening, was developed to produce a friction stir-welded (FSW) Al-alloy joint. The Al-Cu sheets were FSW under different welding parameters and then were plastic-deformed. The microstructural evolution and mechanical properties of the FSW joint were investigated by scanning electron microscopy and tensile tests. It was found that high heat input during FSW and low solution temperature suppress the abnormal grain growth (AGG) of the joint due to the differential in grain size and grain boundary energy. The microstructure heterogeneity of the FSW joint is effectively improved, as no AGG occurs. The retention of fine equiaxed grains and the increase in the density of precipitates result in excellent mechanical properties. The increase in the strength and micro-hardness of the joint mainly depends on the plastic deformation prior to aging treatment.

Keywords abnormal grain growth, friction stir welding, mechanical property, plastic deformation

1. Introduction

Due to the tight competition in the automotive industries during the last decades, tailor-welded blanks (TWBs) of aluminum alloys have been tested for producing vehicle body panels and airframes with stamping processes (Ref 1). The technology joins together sheet products and then subject to the stamping operation to create the parts, which results in reducing vehicle weight and saving cost. It is reported that the TWBs are severely deformed during stamping, and the aluminum alloy joints are always cracked (Ref 2). The poor formability of weld materials is the weak point of TWBs technology.

Friction stir welding (FSW) is a process that has been recently applied to aluminum TWBs. It has shown the potential to produce a high-quality weld (Ref 3). Doley et al. (Ref 4) reported that friction stir-welded TWBs exhibited the higher formability and lower defects than those made with conventional joining processes. Hovanski et al. (Ref 5) demonstrated that aluminum TWBs could be fabricated by FSW at speeds appropriate for automotive manufacturing. Aluminum alloys were welded by FSW in the naturally aged and peak-aged conditions, which were always used in the as-welded condition. Welding optimization for FSW was investigated thoroughly, in terms of mechanical behavior and material flow (Ref 6-8). The

investigations aimed to reduce defects and improve the strength of joints and thus avoided deformation and fractures during service. However, the concerns were totally different for the industrial application of TWBs. The formability of the joints during forming and the strength of the joints after heat treatment were of the greatest concern, as reported by Merklein et al. (Ref 9). Nandan et al. (Ref 10) reviewed advances in the FSW process, weldment structure, and properties, which showed that the majority of the data available on the elongations of FSW joints were below 50% of those of the base material (BM). It was difficult to meet the formability requirements of the TWBs for the automotive industrial application. Hu et al. (Ref 11) explained that the heterogeneous microstructure distribution of the joints led to non-uniform deformation and consequently reduced the formability of the FSW joints.

Post-weld heat treatment (PWHT), as an effective way to improve the formability and strength of the FSW joints, has been widely investigated. Elangovan et al. (Ref 12) proved that the lost strength of the joint could be recovered to 80-90% of that of the BM by PWHT, but the formability of the joints decreased sharply due to abnormal grain growth (AGG) during PWHT. In particular, the small equiaxed grains were more unstable for the deformed FSW joints (Ref 13-15). The rolled FSW joint showed obvious AGG during PWHT (Ref 13) and hot working (Ref 15) and exhibited a significant decrease in the elongation, even in the presence of small Al₃Zr dispersoid particles (Ref 14). Mironov et al. (Ref 16) reported that the deformation induced by the FSW tool was the main reason for the occurrence of AGG. Although AGG could be controlled by welding process optimization, the process window was narrow and the loss in the elongation of the 2095 Al-alloy FSW joint was still significant compared to that of the BM (Ref 17). AGG of the FSW joints damaged the tolerance, structural integrity, and fatigue life of the components. However, at present, many studies about AGG primarily aim to understand the effect of alloy chemistry (Ref 18) and FSW parameters (Ref 19-21) on

Z.L. Hu and **M.L. Dai**, Hubei Key Laboratory of Advanced Technology of Automobile Components, Wuhan University of Technology, Wuhan 430070, People's Republic of China; and Hubei Collaborative Innovation Center for Automotive Components Technology, Wuhan University of Technology, Wuhan 430070, People's Republic of China; and **Q. Pang**, School of Mechanical and Electrical Engineering, Wuhan Donghu University, Wuhan 430212, People's Republic of China. Contact e-mail: pqiuhit@126.com.

the thermal stability of the joint. No information is reported for achieving a full-strength FSW joint in the Al-Cu alloys with no occurrence of AGG during solution treatment.

It is known that TWBs for forming lightweight components are basically connected to one fundamental manufacturing process. First, the Al-alloy sheets are welded and plastic-formed to the required shape and then are heat-treated to strengthen the parts. A new tailor-welded and formed (WF) process is developed to produce a full-strength FSW joint. Al-alloy rolled plates are welded by FSW and then are treated in solution. Following the solution, the joints are deformed and then subjected to age treatments. The new process combines the stages of welding, forming, and heat treatment strengthening, and it is able to produce high-strength integral structures.

2. Experimental Procedure

2024-O aluminum alloy rolled plates with 2.88 mm thickness were welded by FSW. The FSW tool had shoulder diameter of 14 mm and cylindrical tapered pin diameter of 6 mm at top and 4 mm at bottom and 2.88 mm in length. After FSW, the joints were solution at 450 and 495 °C for 40 min and then were quenched in water at 20 °C. Following solution, the joints were plastic-deformed normal to the weld with an elongation of 3-10% and then were subjected to age treatment at 190 °C for 8 h. The whole tailor-welded and formed process is shown in Fig. 1.

After tailor-welded and formed process, the specimens were electrolytically polished in 50 mL HClO₄ + 150 mL C₂H₅OH solution and then were observed under a Zeiss field emission scanning electron microscope (FESEM). The orientation imaging microscopy (OIM) was used to evaluate grain size distribution with step size of 0.2 μm. The micro-hardness test was carried out along the centerlines of the cross sections under a load of 100 g for 10 s. The tensile specimens were prepared according to ASTM B557-02 with a tensile gauge of 30 mm and performed at a crosshead speed of 2 mm/min using an Instron-1186 testing machine.

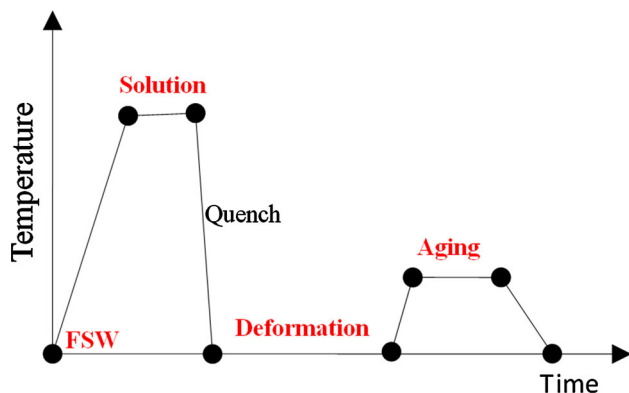


Fig. 1 Schematic of tailor-welded and forming process: FSW-solution-deformation-aging treatment

3. Results and Discussion

3.1 Microstructural Features of FSW Joint

The macrograph results of the as-welded and solution joints (450 and 495 °C) are observed in Fig. 2. No welding defects are detected for any of the joints with different welded parameters. The shape of the weld is apparently dependent on the welding heat input, as the nugget zone (NZ) shows quite a different shape under different welding parameters. The NZ is wider for the joint that experienced high heat input (800 rpm and 100 mm/min). The NZ and thermomechanically affected zone (TMAZ) of the joint are separated by a distinct boundary (as shown by the red circle in Fig. 2). The higher heat input during FSW makes the boundary clearer with different etching contrasts. The refined microstructure is observed in the basin-shaped nugget and shows a typical cross section of an FSW weld.

As expected, AGG occurs in solution at 495 °C for all FSW joints (Fig. 3). A highly refined microstructure has been totally transformed into a coarse-grained structure except for the joint with 800 rpm and 100 mm/min, for which half of the stir zone is stable. It shows neither normal nor abnormal grain growth. The rest of the parts in the stir zone (the upper surface, weld root, and the intersection of the advancing side) show a severe AGG phenomenon. The evolution of the AGG for the FSW joints is illustrated clearly in Fig. 3. The AGG first initiates from the upper surface and then extends to the weld root of the joint, which is proven by the microstructural evolution of the weld with 600 rpm, 300 mm/min and 600 rpm, 100 mm/min after solution at 450 °C. Furthermore, it is revealed that the refined material near the boundary of the advancing side of the weld exhibits low thermal stability due to the occurrence of AGG in the above area. As a result, it is clear that the AGG grows in a downward direction along the intersection of the advancing side and retreating side. As the welding heat input increases, the AGG extends to the center part of the FSW joint during solution. Finally, it consumes the whole weld. It is indicated that the driving force for AGG is the highest at the advancing side neighboring the upper surface (encircled in Fig. 3) and the weld root and at the retreating side adjacent to the weld crown.

It is also revealed that AGG is suppressed entirely for the joints with higher heat input (800 rpm, 100 mm/min) during solution at 450 °C, as shown in Fig. 4. This is completely different from those with lower heat input joints (600 rpm, 300 mm/min and 600 rpm, 100 mm/min). Even after solution at 495 °C for 40 min, the half of the joints with higher heat input present stability, showing neither normal nor abnormal grain growth. It is worth noting that although no AGG occurs in the TMAZ, the grains are also larger than those in the joints with no AGG phenomenon, as shown in Fig. 4.

3.2 Mechanical Features of FSW Joint

Because the FSW joint (800 rpm, 100 mm/min) shows the better thermal stability among the joints, it is chosen for the microstructure and mechanical properties investigation during the tailor-welding and forming process. The micro-hardness of the joints before and after the new process is shown in Fig. 5. The maximum micro-hardness of the as-welded joint is 100% higher than that of the BM. The NZ of the as-welded joint is composed of the recrystallized fine equiaxed grains and exhibits precipitation hardening through a short-term solution followed by natural aging during FSW (Ref 6). Therefore, the

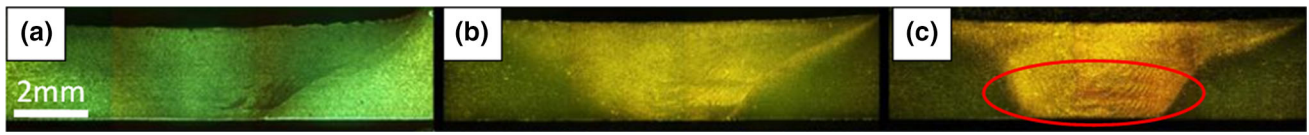


Fig. 2 Macrographs of as-welded joints at different welded parameters, (a) travel speed of 300 mm/min and rotation speed of 600 rpm, (b) travel speed of 100 mm/min and rotation speed of 600 rpm, and (c) travel speed of 100 mm/min and rotation speed of 800 rpm

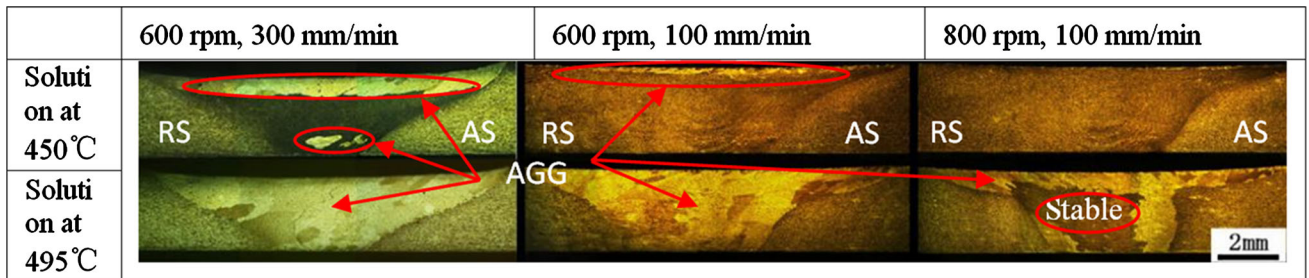


Fig. 3 Macrographs of FSW joints with different welding parameters during solution

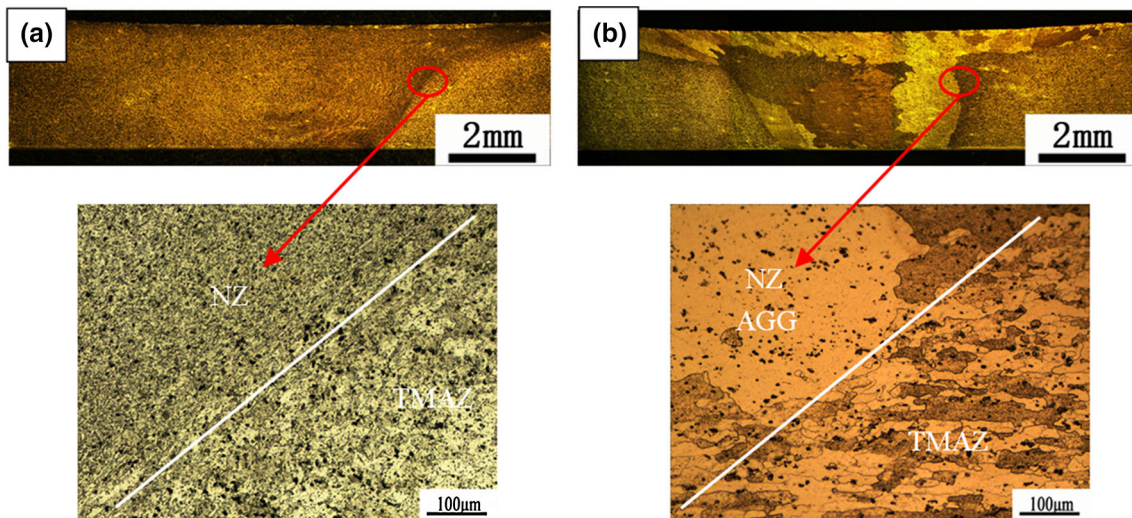


Fig. 4 Micrograph of FSW joints under different solution process, (a) solution at 450 °C, and (b) solution at 495 °C

joint is strengthened by the FSW process. The micro-hardness value in the nugget of the joint (solution at 450 °C and aging without stretch, WF450) is slightly lower than that of the as-welded joint, but the micro-hardness in the TMAZ, HAZ, and BM of the joint are significantly improved. The micro-hardness profiles of the joints are found to be uniform after the new process. This can be attributed to the precipitation hardening through solution followed by artificial aging of the joints.

Figure 5 reveals that the micro-hardness values of joints vary depending on the degree of the deformation. The micro-hardness of the WF 450-3% stretch joint (WF at 450 °C with a 3% cold stretching and aging) is about 120 HV, which is slightly higher than that of the WF 450 joint. The micro-hardness values of the WF joints increase with increasing amounts of cold stretching after solution at 450 °C. The micro-hardness value of the WF 450-10% stretch joint (WF at 450 °C with a 10% cold stretching and aging) is about 140 HV, which is the same as that of the BM-T6.

The tensile properties of FSW joints are shown in Fig. 6. The tensile and yield strengths of WF450 joints are 361 and 183 MPa, respectively, which are 1.7 and 1.9 times higher than those of as-welded joints. However, the strength of the joint after WF at 450 °C still exhibits a significant decrease when compared to that of the BM with T6 temper, whose tensile and yield strengths are 430 and 292 MPa, respectively. The strength of the joints has been significantly improved with an intermediate stretch between solution and aging, and the strength of the joints increases with increasing deformation, especially the yield strength, which increases exponentially. The maximum tensile and yield strengths of the joint are 424 and 392 MPa, respectively, after WF at 450 °C with a stretch of 10% (WF450-10% joint). The tensile strength of the joint is nearly the same as that of BM, but the yield strength of the joint shows a significant increase of 34%. Furthermore, all WF joints show the better elongation than the BM with a T6 temper, as shown in Fig. 6.

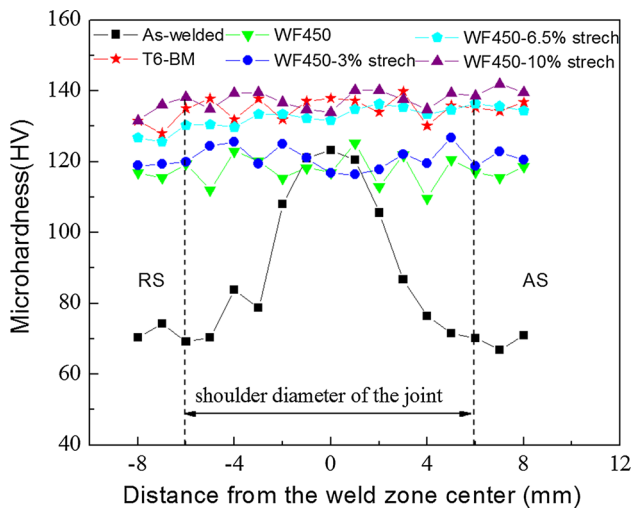


Fig. 5 The micro-hardness distribution of the FSW joints before and after tailor-welded and forming process (WF) process, WF450 joint means solution at 450 °C and aging without stretch, WF 450-3% joints means WF at 450 °C with a 3% cold stretching and aging and so on

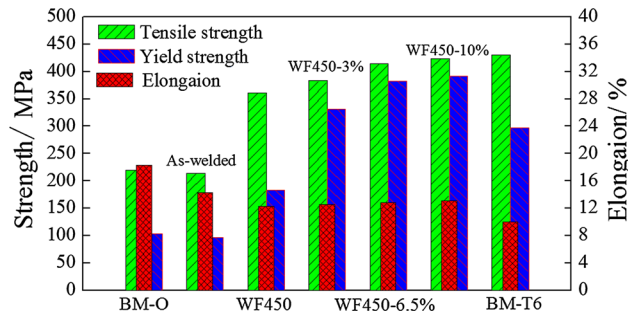


Fig. 6 Tensile properties of the joints before and after tailor-welded and forming process (WF) process, WF450 joint means solution at 450 °C and aging without stretch, WF 450-3% joints means WF at 450 °C with a 3% cold stretching and aging and so on

4. Discussion

4.1 Microstructure Governing AGG Characteristic

AGG is a complex phenomenon, the nature of which is not completely clear (Ref 21). Typical EBSD maps of the FSW joint (800 rpm, 100 mm/min) are shown in Fig. 7. The grain size decreases from top to bottom in the nugget of as-welded joints for experiencing different deformations and temperatures (Fig. 7a). The border initial grain size distribution is expected to contribute a larger thermodynamic driving force for AGG. Moreover, the grains in the upper surface of the as-welded joint contain a high density of sub-boundaries, as shown in Fig. 7(b). The FSW shoulder imparts additional strain into the upper surface of the weld. This may promote the formation of extensive low-angle boundaries (LABs); therefore, the recrystallization microstructure (high-angle boundaries, HABs) is small. Humphreys et al. proved that lower-boundary misorientation possessed lower energy and mobility (Ref 22); correspondingly, higher boundary energy and mobility promoted the preferential growth of abnormal grains. Therefore, AGG initiates from the upper surface, as shown in Fig. 3. A similar

result can be also observed in the bottom region of the joints, which shows a larger fraction of sub-boundaries. This substructure merges into the sub-grains, which are apt to grow into AGG during solution. Therefore, the AGG phenomenon is more pronounced as the solution temperature increases.

The grain size gradient along the thickness of the joint (800 rpm, 100 mm/min) is almost eliminated after WF at 450 °C (Fig. 8a). The fine equiaxed grains are retained in the nugget with size slightly larger than those in the as-welded joints. No AGG can be observed. Furthermore, the grains of the WF joint contain a low density of sub-boundaries in the weld as shown in Fig. 8(b). The experimental results indicate that a uniform microstructure consisting of fine grains in the NZ of the joints diminishes the possibility of AGG. It is deduced that the differentials of grain size in the weld decrease with decreasing grain boundary energy according to the Humphreys model (Ref 22). Therefore, the driving force for AGG during solution could be reduced by promoting continuous grain growth. It is indicated that the occurrence of AGG can be attributed to the presence of gradient grain size and grain boundaries with dissimilar strain gradients in the weld. It is also speculated that decreasing the differentials of grain size and the ratio of the LABs for the FSW joint is an effective way to avoid AGG, even in the presence of grain-size gradients for the as-welded joint.

Figure 9 shows the grains and precipitate particles in the NZ of the WF450 joint (800 rpm, 100 mm/min), which is another key microstructural characteristic that should be considered within a microstructure for AGG. It is reported that the heterogeneous dissolution of unstable particles leads to a non-uniform reduction in the pinning force, which activates the preferential growth of abnormal grains (Ref 21). This approach can be applied successfully for the analysis of AGG in FSW joints, as reported by Hassan et al. (Ref 23). The grains in the NZ of the WF joint are fine and equiaxed, as shown in Fig. 9. The majority of the precipitate particles are located at the grain boundaries in the NZ of WF joints. These particles are compounds of Al-Cu-Mg by energy-dispersive spectrometry analysis. According to the literature, these rod- or lath-shaped compounds with grain sizes of 100-300 nm are strengthening precipitates Al_2CuMg , as investigated by Charlie (Ref 24). It is reported that dispersed, thermally stable precipitates may help to hinder the grain boundaries' migration and prevent AGG (Ref 19). Consequently, these nanometer-scale Al_2CuMg particles tend to precipitate on the grain boundary, and the joints show no sign of AGG during WF.

4.2 Microstructure Governing Mechanical Characteristic

To understand the mechanical property evolution of the FSW joints during WF, it is necessary to consider the second-phase particles of the joints, as shown in Fig. 10, which provides useful information regarding the role and contribution of the microstructural features governing the strength of the joints. It is reported that strengthening precipitates may coarsen or dissolve during FSW, whereas particles, including Fe and Mn, are insoluble in aluminum alloys (Ref 25). All the particles in the SEM image after WF are undissolved Al_2CuMg and insoluble (Cu, Fe, Mn) Al_6 particles, as shown in Fig. 10. The reduction in the precipitate is expected because the solution temperature (450 °C) is lower than the recommended solution temperature (Fig. 10a). The density of the strengthening precipitates in the NZ of the joints is nearly the same as that

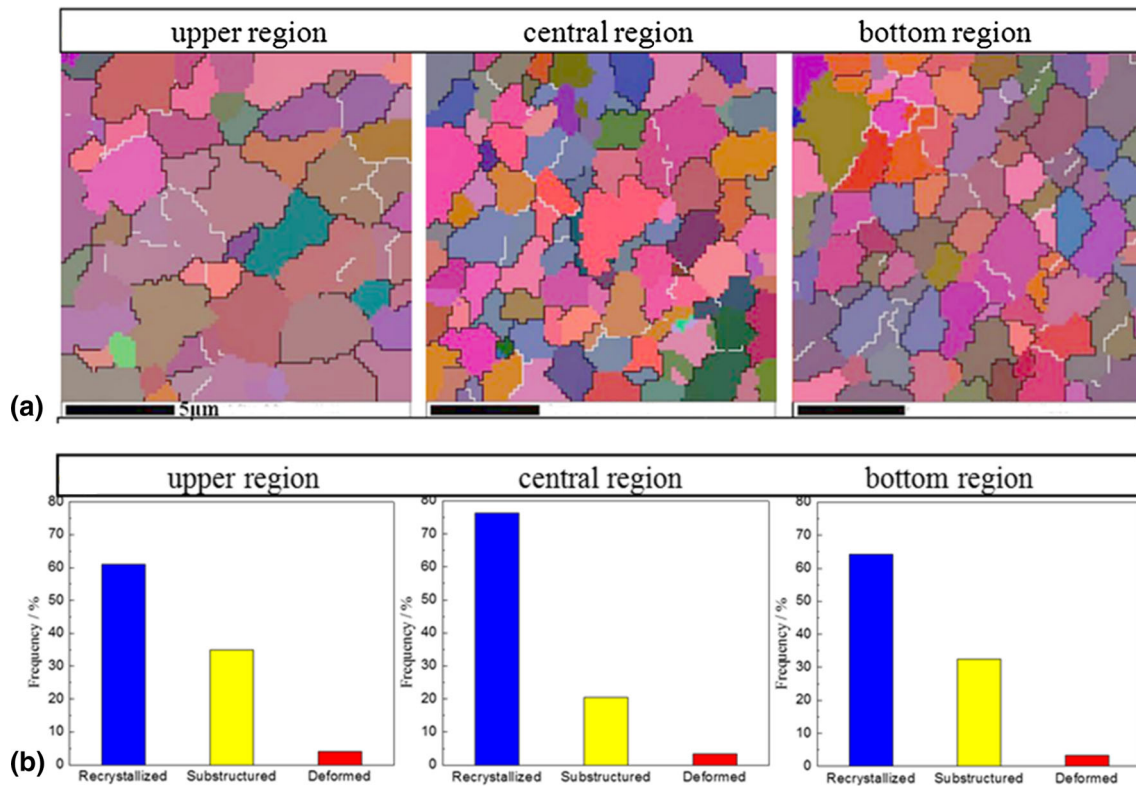


Fig. 7 Microstructure characteristic of the as-welded joint (800 rpm, 100 mm/min), (a) typical EBSD map, and (b) special microstructure distribution

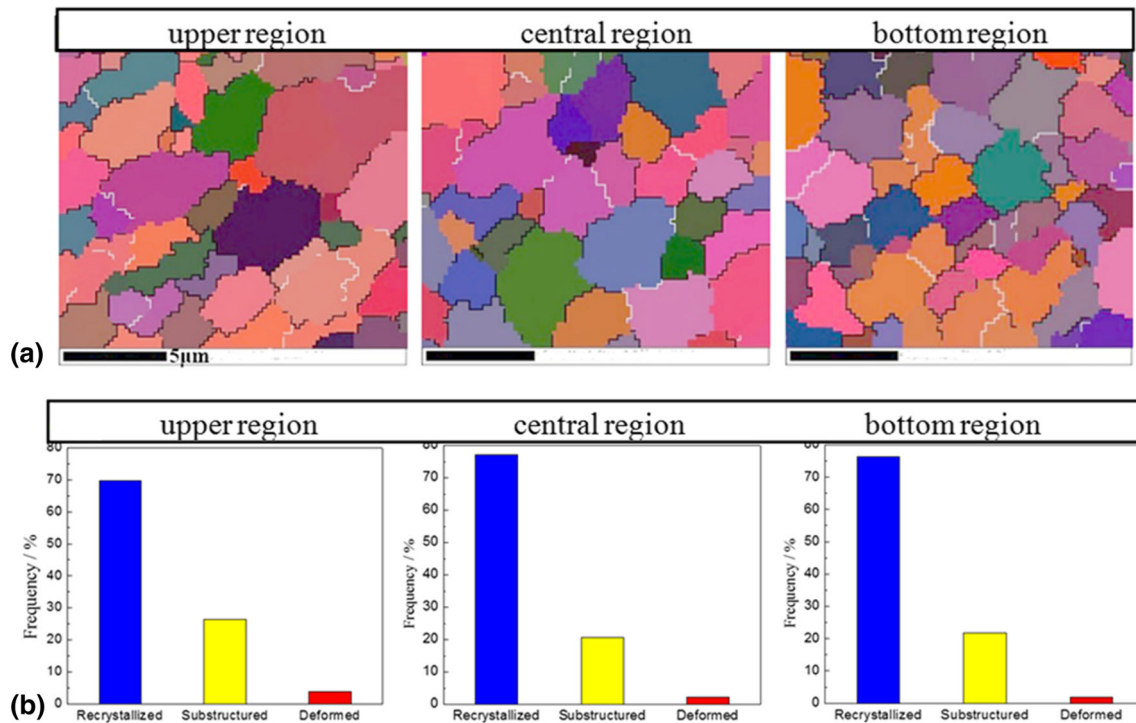


Fig. 8 Microstructure characteristic of the WF450 joint (800 rpm, 100 mm/min), (a) Typical EBSD map, and (b) special microstructure distribution

in the NZ of as-welded joints. Consequently, the micro-hardness values in the NZ for the two joints are similar. The tensile strength of WF joints (450 °C) is only 83% that of the

BM with a T6 temper, even though no AGG occurs in the nugget, which proves that the micro-hardness and strength of the precipitation-hardening aluminum alloys greatly depend on

the precipitate distribution. It should be noted that the NZ of the WF joint experiences an incomplete solution and artificial aging treatment, similar to the NZ of the as-welded joint. The NZ of the as-welded joints also undergoes solution treatment due to the temperature increase during FSW, which results in the partial or complete dissolution of precipitate particles.

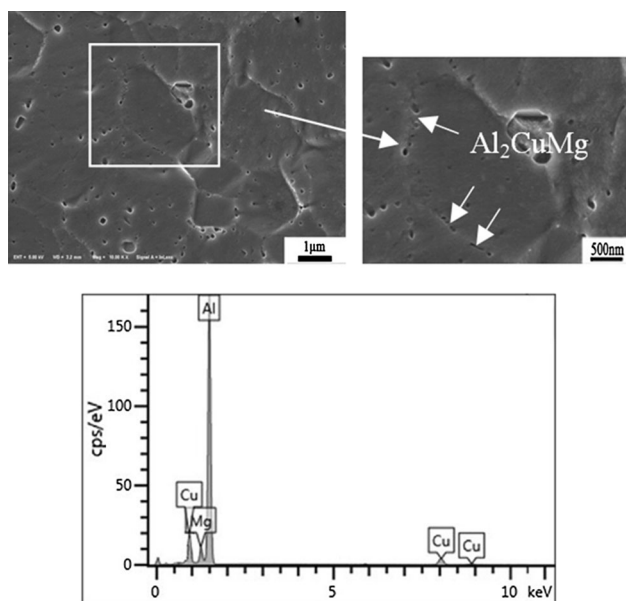


Fig. 9 Secondary electron SEM images of the NZ in the WF450 joints (800 rpm, 100 mm/min)

However, the cooling rate following FSW is not high enough to cause re-precipitation of the dissolved solute (Ref 25).

An obvious increase in the second-phase particles in the nugget can be observed for the WF joint with a stretch of 10% (Fig. 10d). Clearly, the intermediate stretch between solution and aging improves the most important factors for strength, including the density and distribution of the second-phase particles. A large number of vacancies and dislocations are formed during the deformation after solution, which is beneficial for the re-precipitation of fine metastable Al_2CuMg particles during the aging process. The partial dissolution of large precipitates and the formation of fine precipitates take place consecutively in the artificial aging process. Consequently, a uniform dispersion of nanoscale precipitates in the Al-alloy matrix is formed during WF, which can effectively improve the strength of the joints. The improvement in the strength of the joints can be mainly attributed to refinement of the precipitates. These precipitates can act as effective obstacles against the dislocations and enhance the hardness and mechanical strength of the joints. In addition, fine equiaxed grains are reserved in the nugget, which are beneficial to enhancing the mechanical properties of the joints. Therefore, it can be deduced that the fine equiaxed grains and the high density of precipitates play important roles in increasing in the strength of the joints. It is pertinent to point out that the new WF process not only improves the strength, but also enhances the elongation of the joint (Fig. 6). Mahoney et al. (Ref 26) reported that the solution and aging treatment degraded the ductility of the FSW joints, which was mainly caused by the coarsening of precipitate particles and AGG. The microstructural observations (Fig. 9 and 10) reveal that neither the coarsening of precipitates nor the formation of AGG occurs

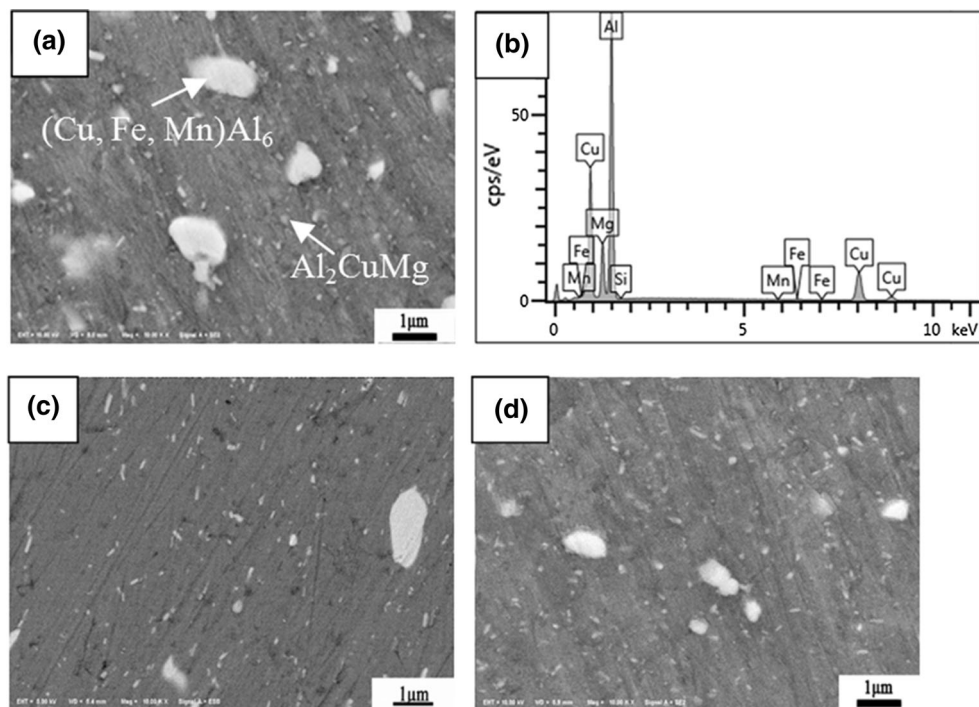


Fig. 10 Backscattered SEM images of the NZ for the joints (800 rpm, 100 mm/min), (a) T6 treatment at 450 °C, (b) EDS spectra for the (Cu, Fe, Mn) Al_6 particles, (c) as-welded, and (d) WF at 450 °C with a 10% stretching

during the WF process. Therefore, all FSW joints show high relative elongation, as shown in Fig. 6.

5. Conclusions

The microstructural evolution and mechanical properties of FSW joint during WF are investigated, and the following conclusions are obtained:

1. The new WF process includes FSW and solution at 450 °C, followed by plastic deformation and artificial aging. A full-strength FSW joint of Al-Cu alloy with no AGG phenomenon is obtained.
2. High heat input during FSW and a low solution temperature are proven to suppress the occurrence of AGG in the NZ. In addition, the Al₂CuMg particles tend to precipitate on the grain boundary, which helps to hinder the migration of the grain boundaries and to prevent the occurrence of AGG.
3. The micro-hardness values of WF joints are uniform. The maximum micro-hardness of the WF joint with a 10% cold stretch is nearly the same as that of the BM with T6 temper.
4. The new WF process can significantly improve the strength of the joints. The tensile strength of the joint is nearly the same as that of BM-T6, and the yield strength of the joint shows an increase of 34%. The increase in the strength of the WF joint mainly depends on the intermediate plastic deformation between solution and aging.

Acknowledgments

This study is financially supported by National Natural Science Foundation of China (51405358, 51775397), China Automobile Industry Innovation and Development Joint Fund (U1564202), the 111 Project (B17034) and Open Fund of Shanghai Key Laboratory of Digital Manufacture for Thin-Walled Structures. The authors would like to take this opportunity to express their sincere appreciation.

References

1. P.L. Threadgill, A.J. Leonard, H.R. Shercliff, and P.J. Withers, Friction Stir Welding of Aluminium Alloys, *Int. Mater. Rev.*, 2009, **54**, p 49–93
2. X.S. Wang, Z.L. Hu, S.J. Yuan, and L. Hua, Influence of Tube Spinning on Formability of Friction Stir Welded Aluminum Alloy Tubes for Hydroforming Application, *Mater. Sci. Eng. A*, 2014, **607**, p 245–252
3. S.J. Yuan, Z.L. Hu, and X.S. Wang, Evaluation of Formability and Material Characteristics of Aluminum Alloy Friction Stir Welded Tube Produced by a Novel Process, *Mater. Sci. Eng. A*, 2012, **543**, p 210–216
4. J.K. Doley and S.D. Kore, A Study on Friction Stir Welding of Dissimilar Thin Sheets of Aluminum Alloys AA 5052–AA 6061, *ASME J. Manuf. Sci. Eng.*, 2016, **138**, p 114502
5. Y. Hovanski, P. Upadhyay, J. Carsley, and T. Luzanski, High-Speed Friction-Stir Welding to Enable Aluminum Tailor-Welded Blanks, *JOM*, 2015, **67**, p 1045–1053
6. H. Aydın, A. Bayram, and I. Durgun, The Effect of Post-weld Heat Treatment on the Mechanical Properties of 2024-T4 Friction Stir-Welded Joints, *Mater. Des.*, 2010, **31**, p 2568–2577
7. F.F. Mustafa, A.H. Kadhym, and H.H. Yahya, Tool Geometries Optimization for Friction Stir Welding of AA6061-T6 Aluminum Alloy T-Joint Using Taguchi Method to Improve the Mechanical Behavior, *ASME J. Manuf. Sci. Eng.*, 2015, **137**, p 031018
8. Z.L. Hu, X.S. Wang, Q. Pang, F. Huang, X.P. Qin, and L. Hua, The Effect of Post-processing on Tensile Property and Microstructure Evolution of Friction Stir Welding Aluminum Alloy Joint, *Mater. Charact.*, 2015, **99**, p 180–187
9. M. Merklein, M. Johannes, M. Lechner, and A. Kuppert, A Review on Tailored Blanks-Production, Applications and Evaluation, *J. Mater. Process. Technol.*, 2014, **214**, p 151–164
10. R. Nandan, T. DebRoy, and H.K.D.H. Bhadeshia, Recent Advances in Friction-Stir Welding-Process, Weldment Structure and Properties, *Prog. Mater. Sci.*, 2008, **53**, p 980–1023
11. Z.L. Hu, S.J. Yuan, and X.S. Wang, Quantitative Investigation of the Tensile Plastic Deformation Characteristic and Microstructure for Friction Stir Welded 2024 Aluminum Alloy, *Mater. Charact.*, 2012, **73**, p 114–123
12. K. Elangovan and V. Balasubramanian, Influences of Post-weld Heat Treatment on Tensile Properties of Friction Stir-Welded AA6061 Aluminum Alloy Joints, *Mater. Charact.*, 2008, **59**, p 1168–1177
13. S.J. Yuan, Z.L. Hu, and X.S. Wang, Formability and Microstructural Stability of Friction Stir Welded Al Alloy Tube During Subsequent Spinning and Post Weld Heat Treatment, *Mater. Sci. Eng. A*, 2012, **558**, p 586–591
14. S. Katsas, R. Dashwood, M. Jackson, and R. Grimes, Influence of Subsequent Cold Work on the Superplastic Properties of a Friction Stir Welded Aluminium Alloy, *Mater. Sci. Eng. A*, 2010, **527**, p 1022–1026
15. S. Mironov, K. Masaki, Y.S. Sato, and H. Kokawa, Relationship Between Material Flow and Abnormal Grain Growth in Friction-Stir Welds, *Scr. Mater.*, 2012, **67**, p 983–986
16. D.H. Ko, J.H. Kim, D.C. Ko, and B.M. Kim, Improvement of Weldment Properties by Hot Forming Quenching of Friction Stir Welded TWB Sheet, *Adv. Mech. Eng.*, 2014, **6**, p 1–9
17. M.M. Attallah and H.G. Salem, Friction Stir Welding Parameters: A Tool for Controlling Abnormal Grain Growth During Subsequent Heat Treatment, *Mater. Sci. Eng. A*, 2005, **391**, p 51–59
18. M.A. Garcia-Berna, R.S. Mishra, and H.D. Verma, Inhibition of Abnormal Grain Growth During Hot Deformation Behavior of Friction Stir Processed 5083 Al Alloys, *Mater. Sci. Eng. A*, 2015, **636**, p 326–330
19. I. Charit and R.S. Mishra, Abnormal Grain Growth in Friction Stir Processed Alloys, *Scr. Mater.*, 2008, **58**, p 367–371
20. G. Ipekoglu, S. Erim, and G. Cam, Effects of Temper Condition and Post Weld Heat Treatment on the Microstructure and Mechanical Properties of Friction Stir Butt-Welded AA7075 Al Alloy Plates, *Int. J. Adv. Manuf. Technol.*, 2014, **70**, p 201–213
21. K.S. Suresh, A.D. Rollett, and S. Suwas, Evolution of Microstructure and Texture During Deformation and Recrystallization of Heavily Rolled Cu-Cu Multilayer, *Metall. Mater. Trans. A*, 2013, **44**, p 3866–3881
22. F.J. Humphreys, *Proceedings of the Grain Growth in Polycrystalline Materials III*, H. Weiland, B.L. Adams, and A.D. Rollett, Eds., TMS, Warrendale, PA, 1998, p 13–22
23. K.A.A. Hassan, A.F. Norman, D.A. Price, and P.B. Prangnell, Stability of Nugget Zone Grain Structures in High Strength Al-Alloy Friction Stir Welds During Solution Treatment, *Acta Mater.*, 2003, **51**, p 1923–1936
24. C. Brooks and R. Charlie, *Heat Treatment, Structure and Properties of NonFerrous Alloys*, ASM International, Metals Park, OH, 1987, p 112–114
25. M.J. Starink, A. Deschamps, and S.C. Wang, The Strength of Friction Stir Welded and Friction Stir Processed Aluminium Alloys, *Scr. Mater.*, 2008, **58**, p 377–382
26. M.W. Mahoney, C.G. Rhodes, J.G. Flintoff, W.H. Bingel, and R.A. Spurling, Properties of Friction Stir Welded 7075 T651 Aluminum, *Metall. Mater. Trans. A*, 1998, **29**, p 1955–1964